










Single-lined Spectroscopic Binary Star Candidates from a Combination of the RAVE and *Gaia* DR2 Surveys

Danijela Birko¹ , Tomaž Zwitter¹ , Eva K. Grebel², Quentin A Parker^{3,4}, Georges Kordopatis⁵ , Joss Bland-Hawthorn⁶ , Kenneth Freeman⁷, Guillaume Guiglion⁸ , Brad K. Gibson⁹ , Julio Navarro¹⁰, Warren Reid^{11,12}, G. M. Seabroke¹³, Matthias Steinmetz⁸ , and Fred Watson¹⁴

¹ University of Ljubljana, Faculty of Mathematics and Physics, Ljubljana, Slovenia; danijela.birko@gmail.com

² Astronomisches Rechen-Institut, Zentrum für Astronomie der Universität Heidelberg, Mönchhofstr. 12–14, D-69120 Heidelberg, Germany

³ CYM Physics Building, The University of Hong Kong, Pokfulam, Hong Kong, SAR, People' Republic of China

⁴ The Laboratory for Space Research, Hong Kong University, Cyberport 4, Hong, Kong, SAR, People' Republic of China

⁵ Université Côte d'Azur, Observatoire de la Côte d'Azur, CNRS, Laboratoire Lagrange, France

⁶ Institute of Astronomy, School of Physics, University of Sydney, Australia

⁷ RSCA Australian National University, Canberra, Australia

⁸ Leibniz-Institut für Astrophysik Potsdam (AIP), An den Sternwarte 16, D-14482 Potsdam, Germany

⁹ Jeremiah Horrocks Institute for Astrophysics & Super-computing, University of Central Lancashire, Preston, UK

¹⁰ CIFAR Fellow, University of Victoria Physics and Astronomy, Victoria, BC V8P 5C2, Canada

¹¹ Department of Physics and Astronomy, Macquarie University, Sydney, NSW 2109, Australia

¹² Western Sydney University, Locked bag 1797, Penrith South, NSW 2751, Australia

¹³ Mullard Space Science Laboratory, University College London, Holmbury St Mary, Dorking, RH5 6NT, UK

¹⁴ Anglo-Australian Observatory, Sydney, Australia

Received 2019 June 20; revised 2019 July 24; accepted 2019 August 6; published 2019 September 23

Abstract

The combination of the final version of the Radial Velocity Experiment (RAVE) spectroscopic survey data release 6 with radial velocities (RVs) and astrometry from *Gaia* DR2 allows us to identify and create a catalog of single-lined binary star candidates (SB1), their inferred orbital parameters, and to inspect possible double-lined binary stars (SB2). A probability function for the detection of RV variations is used for identifying SB1 candidates. The estimation of orbital parameters for main-sequence dwarfs is performed by matching the measured RVs with theoretical velocity curves sampling the orbital parameter space. The method is verified by studying a mock sample from the SB 9 catalog. Studying the boxiness and asymmetry of the spectral lines allows us to identify possible SB2 candidates, while matching their spectra to a synthetic library indicates probable properties of their components. From the RAVE catalog we select 37,664 stars with multiple RV measurements and identify 3838 stars as SB1 candidates. Joining RAVE and *Gaia* DR2 yields 450,646 stars with RVs measured by both surveys and 27,716 of them turn out to be SB1 candidates, which is an increase by an order of magnitude over previous studies. For main-sequence dwarf candidates we calculate their most probable orbital parameters: orbital periods are not longer than a few years and primary components have masses similar to the solar mass. All our results are available in the electronic version.

Key words: binaries: spectroscopic – methods: data analysis – surveys

Supporting material: machine-readable tables

1. Introduction

The majority of stars are members of multiple systems of two or more gravitationally bound stars. In the vast majority of cases these stars are coeval and have an identical chemical composition, and in favorable cases their masses and/or sizes can be determined directly. Yet, in the majority of systems with orbital periods of weeks to years it is a challenge even to identify their multiple nature. Detection of variability of radial velocities (RVs) is a very successful, though a relatively time-consuming method, which has been extensively used in studies of dwarfs and sub-dwarfs (Duquennoy & Mayor 1991; Fischer & Marcy 1992), massive binary systems (e.g., Sana et al. 2009), and binary stars in clusters (Abt & Willmarth 1999; Sommariva et al. 2009). There have been several surveys dedicated to the search of spectroscopic binaries (e.g., Latham et al. 2002; Griffin 2006; Mermilliod et al. 2007). The Geneva–Copenhagen Survey (Nordström et al. 2004) marked a milestone in the size of the sample, as it presented ~ 5 RV measurements of 14,139 F- and G-type dwarfs drawn from a kinematically unbiased magnitude-limited sample, painstakingly observing one star at a time. A landmark result of this

effort was the realization that spectroscopic binarity can be detected in 19% of the observed targets, while the fraction of binary stars of all types reached 34%, in agreement with an earlier result of Duquennoy & Mayor (1991).

The last decade has been marked by much larger ground-based spectroscopic surveys, which use wide-field coverage and fiber optics to obtain spectra of a hundred or more stars at a time. The results are not only RVs but also spectroscopically determined values of stellar parameters, including chemistry. On the other hand, the scientific focus is shifting from stellar kinematics to Galactic archaeology, so the goal is to observe as many stars as possible. This means that most targets are observed only during a single night, with the majority of repeated observations consisting of two visits per target scheduled days to years apart. So any statement on binarity from these spectroscopic surveys is based on a large number of targets with a small number of visits. These properties are typical for the Radial Velocity Experiment (RAVE) survey (Steinmetz et al. 2006), but also for *Gaia*-ESO (Gilmore et al. 2012), Apache Point Observatory Galactic Evolution Experiment (APOGEE; Holtzman et al. 2015), The Large Sky Area

Multi-object Fiber Spectroscopic Telescope (LAMOST; Liu et al. 2017), and The GALactic Archaeology with HERMES (GALAH; De Silva et al. 2015) surveys.

Here we focus on spectroscopic binaries that can be identified in the RAVE survey. Double-lined binaries (SB2) where we identify both sets of spectral lines are quite rare (Matijević et al. 2012), as they imply a very similar mass of both components. Another major reason why SB2 are rare is that the geometry needs to be rather favorable for us to see the line split. So our primary goal is to identify single-lined binaries (SB1), binaries where only spectral lines of primary components can be detected, which are much more common. We base our approach on an earlier study (Matijević et al. 2011), but with two important upgrades: (i) our analysis is based on the final and complete set of RAVE spectra (M. Steinmetz et al. 2019, in preparation) which approximately doubles the considered sample and (ii) RVs derived by RAVE are matched to those of ESA’s *Gaia* space mission (Gaia Collaboration et al. 2018), which increases the sample with multiple measurements by an order of magnitude. A Monte-Carlo approach is used to infer physical properties of the identified SB1 binaries. Their spectra are also searched for the presence of light from a secondary component.

We start with a sample based on RAVE observations only. In Section 2 we present the data and in Section 3 we summarize the method to select SB1 candidates. Next, we present basic properties of the SB1 sample, statistical inference of values of fundamental parameters, and results of the search for absorption lines from a secondary component. In Section 7 we repeat the whole process, now including also RV observations from the *Gaia* satellite which are, however, different enough from the RAVE observations to keep their analysis separate from the one using RAVE observations only. Finally we add some discussion of the results and an outline for the future.

2. RAVE Observations and Sample Selection

RAVE (Steinmetz et al. 2006; Zwitter et al. 2008; Siebert et al. 2011; Kordopatis et al. 2013; Kunder et al. 2017; M. Steinmetz et al. 2019, in preparation) is a medium resolution ($R \sim 7500$) spectroscopic survey of the Milky Way. It used the UK Schmidt telescope at the Australian Astronomical Observatory to obtain over half a million stellar spectra over the period of 2003 April 12 to 2013 April 4. These cover a wavelength range of 8410–8795 Å. The survey properties as well as all its data products and analysis are described in detail in its final data release paper (M. Steinmetz et al. 2019, in preparation). Here we provide just a brief summary as a service to the reader.

RAVE is the first systematic (wide-field coverage) spectroscopic Galactic archaeology survey. While the survey is ongoing, its goals were gradually surpassing its original name by supplementing determination of RV with estimates of effective temperature, surface gravity, and chemical properties, including abundances of aluminum, iron, magnesium, silicon, titanium, and nickel in the stellar photospheres (these abundances are quoted in order of increasing uncertainties, which generally range from 0.14 to 0.23 dex). An inclusive approach has been used, where information obtained from observed spectra was supplemented with complementary photometric and astrometric information, as it became available.

The final RAVE data release contains 518,392 spectra of 451,788 stars, which present a magnitude-limited sample with

$9 < I < 12$. The typical signal-to-noise ratio (S/N) of the measured spectra is ~ 40 per pixel. The RAVE wavelength range matches that of the *Gaia* mission. This wavelength range includes a lot of spectral lines, most importantly the singly ionized calcium triplet ($\lambda\lambda = 8498, 8542, 8662$ Å), the Paschen series of hydrogen, and Fe I multiplets. In the measured part of the spectrum, contributions from telluric lines can be neglected and the only significant spectral signature of the interstellar medium is the diffuse interstellar band at 8620 Å (Munari et al. 2008; Kos et al. 2014).

The selection of the RAVE targets was very close to a random magnitude-limited sample of southern stars, but avoiding fields closer than ~ 5 degrees from the Galactic plane and those in the direction of the Galactic bulge. Details of the selection function are discussed in Wojno et al. (2017). A random selection implies that some of the stars belong to rare spectral types or brief evolutionary stages. Local linear embedding was shown to be an efficient morphological classification technique to pinpoint such peculiar cases and has been applied to RAVE (Matijević et al. 2012). While morphological classification proved efficient in detecting SB2 objects and chromospherically active stars it is clear that it cannot identify SB1 stars, which are hidden among the vast majority of 90%–95% of stars with morphologically normal spectra.

The derivation of RVs is the main result of interest to us here. Velocities are derived as described in Siebert et al. (2011). A two stage process is used. First a rough estimate of RV, with a typical precision better than 5 km s^{-1} , is obtained using a subset of 10 template synthetic spectra covering a wide range of stellar parameters. Next, a best-matching template is constructed using the full template database with a penalized chi-square technique described in Zwitter et al. (2008). This template then allows us to determine the final, more precise RV, which is corrected for possible zero-point shifts (due to thermal instabilities of the instrument) and reported in the inertial frame of the Solar barycenter. As discussed in M. Steinmetz et al. (2019, in preparation), the typical error of the derived RV in the RAVE survey is $\sim 1.1 \text{ km s}^{-1}$.

SB1s can be identified from multiple RV measurements of good quality, so we used the following selection criteria:

1. to safeguard against systematic problems with measurements of noisy spectra we used only those with a $\text{SNR}_{\text{avg_SPARV}} \geq 20$ in RAVE DR6;
2. only stars that have all their spectra classified as normal (flag1 with the value “n”) were used in RAVE DR6; and
3. only stars with at least two RV determinations were considered.

The first criterion is fulfilled for 414,637 (91.8%) stars and the second further narrows selection to 395,919 (87.4%) stars in RAVE DR6. The third criterion is more selective, though unavoidable in a search of SB1 candidates. In total 47,360 stars (9.1%) have multiple observations. When applying the other two criteria we end up with a sample of 37,661 stars with repeated observations. Some of the targets have been observed up to 13 times (Figure 1). Most of the stars with at least six visits are located at Galactic latitude $b > 30^\circ$ and are part of a logarithmic cadence with observations separated by approximately 1, 4, 10, 40, 100, and 1000 days. But a vast majority of stars have only two spectra, form a random subsample of the RAVE survey, and are of primary interest to us here. Some of

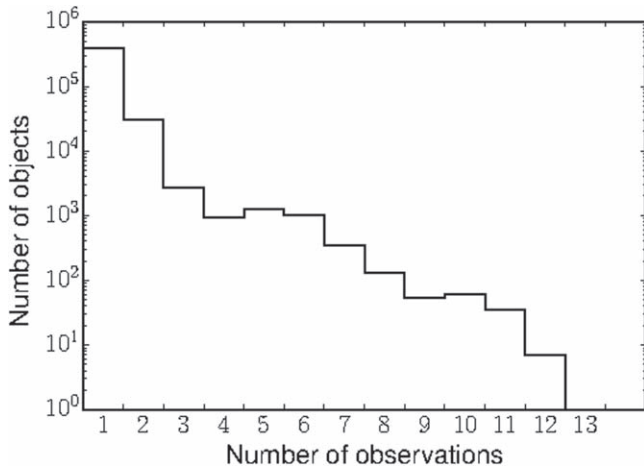


Figure 1. Histogram of the number of RAVE observations per object.

the repeats were made only days apart but about half have a time span longer than 2 yr (Figure 2).

3. The Method

The identification of SB1 candidates is based on the detection of their RV variability. So we need a quantitative criterion for considering changes in RV as significant. Following the method and reasoning from Matijevič et al. (2011), one can write the probability that RV_2 is larger than RV_1 as

$$P(2 > 1) = \frac{1}{2} \left[1 + \operatorname{erf} \left(\frac{RV_2 - RV_1}{\sqrt{2(\sigma_1^2 + \sigma_2^2)}} \right) \right], \quad (1)$$

where RV_1 and RV_2 are RVs and σ_1 and σ_2 are the errors measured for the same star at the two different observations. The squares of the RV errors σ_i^2 can be treated as variances of the Gaussian distribution with the RV_i as the mean value. If we would pick two samples from each of these distributions, $P(2 > 1)$ represents the probability that the pick from the second sample is greater than the pick from the first one. If the RVs are the same, the numerator of the error function will be zero and the probability will equal one-half. For a pair of very different RVs and comparably small errors, the error function approaches 1, and consequently the complete probability goes to 1. For stars with a significant RV variability the value of P should be close to 1, so we introduce a new function that includes a logarithm of P

$$p_{\log} = -\log_{10}(1 - P). \quad (2)$$

For objects with very significant RV variability the argument of the logarithm can be very small and cause floating point errors, so we limit the value of p_{\log} to 14. Pourbaix et al. (2005) use $p_{\log} = 2.87$ as a lower limit indicating a significant RV variability, assuming equal RV errors. Such a limit on p_{\log} corresponds to RV values that are $4.24\sigma_i$ apart. Similarly, $p_{\log} < 2$ corresponds to RV values less than $3.3\sigma_i$ apart, so the variability is questionable. And $p_{\log} < 1$ implies RV differences smaller than $1.8\sigma_i$, so an insignificant RV variability.

Detection of RV variability is not a sufficient criterion to identify an SB1 object. We want to check if RV variability is

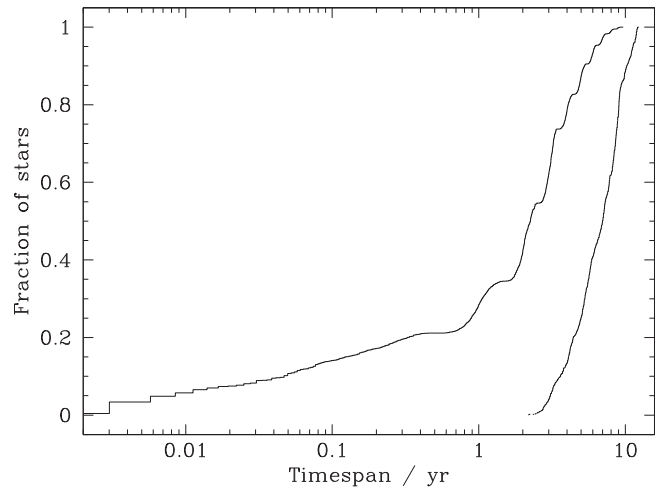


Figure 2. Cumulative plot of a time span between the first and the last observations of the same object within the RAVE survey (left line) and for a combination of RAVE data with RV measurements of *Gaia* (right line). In the latter case the assumed epoch for the *Gaia* observation is 2015 June 15.

Table 1
Number and Fraction of SB1 Candidates for Different Values of p_{\log}

N obs	N	$p_{\log} > 2.87$		$p_{\log} > 4$		$p_{\log} > 6$	
		N	%	N	%	N	%
2	31,059	2384	7.7	1694	5.5	1183	3.8
3	2744	394	14.4	273	10.0	166	6.0
4	943	182	19.3	107	11.3	61	6.5
5	1269	276	21.7	166	13.1	102	8.0
6	1015	326	32.1	210	20.7	106	10.4
7	345	120	34.8	76	22.0	43	12.5
8	131	60	45.8	39	30.0	24	18.3
9	53	23	43.4	16	30.2	8	15.1
10	60	33	55.0	28	46.7	16	26.7
11	35	19	54.3	16	45.7	8	22.9
12	7	3	42.9	2	28.6	0	0.0
≥ 2	37,661	3838	10.2	2627	7.0	1717	4.6

Note. N is the number of objects with N obs observations per object. The fraction of SB1 is higher for a higher number of observations. The longer time span between re-observations of objects with higher N obs results in a higher percentage of SB1s.

not caused by surface activity and if the object shows photometric variability, which is unlikely considering long orbital periods of a majority of SB1 stars. Although we required that spectra of SB1 candidates are morphologically classified as those of normal single stars, we made additional cross-checks. In particular, Žerjal et al. (2013) made a catalog of chromospherically active stars, and photometric variability can be identified using the RAVE DR5 + *Gaia* DR2 photometric variability flag (phot_variable_flag). These checks do not change our results significantly. Among the 3838 candidates discussed in the next section only 3 are known to be chromospherically active and 17 have a flag for photometric variability; most of them are red giants. Also, we checked RV variability as a function of the time span. Close or semi-detached binaries that fill their Roche lobe, with periods usually shorter than one day, have large RV variability. Among SB1 candidates the majority of objects have low RV variability, and 23 objects have RV variability greater than 140 km s^{-1} for different time spans, from one day up to a few years.

Table 2

Representative Extract from the Full List of SB1 Candidates, Reporting the Number of Observations (N obs), their Time Span in Days, and the Epoch of the First and the Last Observation by RAVE

Object	p_{\log}	N obs	Time Span	Epoch (first)	Epoch (last)
J000107.9–412208	4.38	2	1862	2005 Aug 6	2010 Sep 11
J000349.3–405352	4.10	3	1564	2003 Aug 9	2007 Nov 20
J114037.8–260605	3.05	6	123	2009 Jan 27	2009 May 30
J114110.6–320837	6.47	7	1167	2006 Mar 18	2009 May 28
J114155.8–235143	7.00	4	100	2009 Feb 19	2009 May 30

(This table is available in its entirety in machine-readable form.)

4. SB1 Candidates in the RAVE-only Sample

SB1s were searched for in RAVE using the method described above. This is similar to Matijevič et al. (2011) but we applied it to a larger sample. Instead of considering only data obtained up to the third data release we use the sixth and final RAVE data release. This increases the number of SB1 candidates from 1333 to 3838 and keeps their percentage at $\sim 10\%$ of the stars with repeated observations. We note that the fraction of SB1 candidates reaches $\sim 30\%$ for objects with a large number of observations (Table 1). In Table 2 we report the basic properties of our 3838 SB1 candidates. Their individual RV measurements are published by M. Steinmetz et al. (2019, in preparation).

Next we study the physical properties of the primary stars in SB1 candidate systems. Figure 3 shows two peaks in the distribution of the effective temperature, one at ~ 4500 K for the red clump and giant stars with masses larger than $1.5 M_{\odot}$ and another at ~ 6000 K for the main-sequence dwarfs with masses of $\sim 1-1.2 M_{\odot}$. SB1 candidates have a slightly lower metallicity than the general population, maybe due to a contribution from the secondary star spectrum. The S/N of the re-observed stars and SB1s is higher than in the general population because brighter stars are re-observed more frequently than the faint ones in RAVE (so observation time was used more efficiently). The same properties can be seen also in an apparent magnitude histogram. Objects with repeated observations and SB1 candidates have lower magnitudes than the general RAVE sample. As shown in Figure 2, the time span between the first and the last observation of a given object is around 10 yr, so systems with significantly larger orbital periods cannot be detected. This is demonstrated also by Figure 4, which shows that the most probable maximum RV differences are $\sim 5 \text{ km s}^{-1}$, which at our limit of $p_{\log} = 2.87$ corresponds to a pair measurements with uncertainties $\sim 1.2 \text{ km s}^{-1}$, a typical value for RAVE. A slight dependence of the position of the most probable RV differences on stellar type is therefore driven by the fact that giants tend to have their RVs measured with a greater precision, as their spectral lines are numerous and sharper. The maximal RV differences can reach 60 or even 100 km s^{-1} , which should correspond to rather close systems with short orbital periods.

5. Orbital Parameters for Main-sequence Dwarfs

The RV of a binary star is given by the following equation:

$$RV = \frac{2\pi a \sin i}{P\sqrt{1-e^2}} \cdot [\cos(\Theta + \omega) + e \cos \omega] + \gamma, \quad (3)$$

where i is the orbital inclination, e the eccentricity, P the orbital period, Θ the true anomaly, ω the longitude of periastron, γ the

RV of the center of mass, and a the semimajor axis. The latter relates to the mass of the primary star (M_1) and the mass ratio $q = M_2/M_1$ as

$$a = \sqrt[3]{\frac{P^2 GM_1(1+q)}{4\pi^2}} \cdot \frac{q}{1+q}. \quad (4)$$

All six parameters cannot be determined from the small number of re-observations of a given object obtained by RAVE. But for objects with at least four RV determinations well distributed over time one can attempt a probabilistic approach, with the goal of obtaining approximate estimates for their orbital periods. To do so one should adopt a grid of parameter values that are to be tested. These are given in Table 3. We limit our analysis to primary stars on the main sequence, so that we could infer their mass M_1 from their spectroscopically determined effective temperature.

All combinations of these parameters do not occur in nature. Following Duquennoy & Mayor (1991) and Raghavan et al. (2010) we adopt the following constraints:

1. main-sequence systems with $P < 12$ days are assumed to have circular orbits due to tidal interaction in close binaries;
2. systems with a period of $P > 12$ days have a flat distribution in eccentricity that varies from 0.0 to ~ 0.8 , independent of period; and
3. short-period systems ($P < 100$ days) have $q > 0.4$.

There are 406 SB1 candidates with primaries that are main-sequence dwarfs and that have at least four RVs measured by RAVE. This makes them suitable objects to attempt an approximate determination of their orbital periods. To do so, we first split them into four groups according to the sign of their RV changes: in the first group are objects where the RV derivative is either positive or negative throughout ($n = 0$), and in the other three groups are objects with one, two, or more changes in the sign of their RV derivative ($n = 1, 2, >2$). The first two groups are well populated while there are only a handful of objects in the last two groups. These groups can be used to roughly infer what are likely values of P . For the first two groups ($n = 0, 1$) we assumed that P cannot be longer than eight times the time span between the first and the last observation, for the third group ($n = 2$) we lower the maximum period to three times the time span and for the last group ($n > 2$) to within the time span. Next we use these limits on P to compare observed RVs to the calculated ones by marginalizing over other parameters. In particular, for each object we generate 500 sets of randomized values of inclination, longitude of periastron, and initial orbital phase,

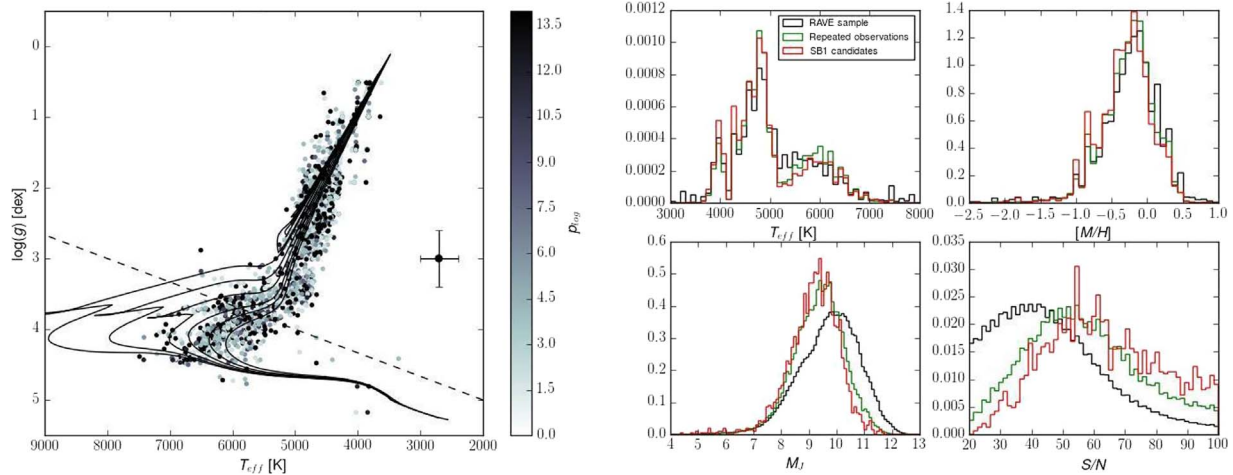


Figure 3. Left panel: Kiel diagram of SB1 candidates, color coded according to p_{\log} values. The dashed line separates main-sequence dwarfs from giant stars. The Padova isochrones plotted as solid lines have solar metallicity and ages of 1–4 Gyr with steps of 1 Gyr. Right panel: histograms of effective temperature (MADERA pipeline), metallicity (MADERA pipeline), magnitude, and S/N show distributions that are generally different for the complete RAVE sample (black), for objects with multiple observations (green), and for SB1 candidates (red).

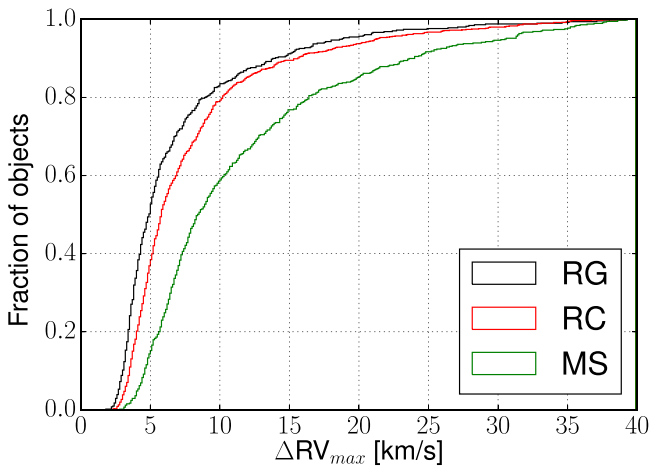


Figure 4. Cumulative histogram of maximum RV changes between measurements for red giant (RG), red clump (RC), and main-sequence (MS) SB1 candidates. This diagram shows that RV variability is the largest for main-sequence stars and the lowest for red giant stars. Main-sequence stars have statistically lower masses, smaller orbits, and consequently larger RV variability in comparison to red giant and red clump stars.

and for each of these sets we check on all allowed combinations of period, eccentricity, and mass ratio, as quoted in Table 3.

The number of parameters is similar or even larger than the number of data points available, so we are not in a position to determine their values. Still, likely ranges of some parameters, such as mass ratio, orbital period, system velocity, and a rough estimate of eccentricity can be judged from our data, so we report these estimates in Table 4. On the other hand the initial orbital phase, longitude of periastron, and inclination are either completely driven by uncertainties in orbital period or they are poorly constrained by the RV nature of our data—so we refrain from reporting them in Table 4. Typical errors on mass of the primary star are determined to within 10% using the effective temperature of the primary and its assumed position on the main sequence. For other values their median value and quartile brackets are reported. The uncertainties are substantial, still we believe such information is useful. For example, it is

clear that J142501.1–290222 is a binary with an orbital period of just a few days and with quite similar masses of the components. The system (γ) velocity is relatively well constrained from derived sets of orbital solutions, so these values may be useful when estimating Galactic orbits of SB1 candidates. Figure 5 illustrates solutions for a few objects.

An SB1 with a very high eccentricity can be very hard to identify. Such a binary spends only a very short time close to periastron at high orbital velocities, but most of the time their RVs are nearly constant and close to the γ velocity of the center of mass. RAVE objects generally have a small number of observations (Figure 1), so it is quite likely to miss the RV spike around the periastron passage and the object might not be identified as a binary at all.

Most of the SB1 candidates have orbital periods shorter than a year, and only $\sim 10\%$ of the objects have orbital periods larger than 2 yr (Figure 6, left panel). As already mentioned, orbital periods cannot be very long as observations span only a few years or less, but they cannot be very short either as large RV variations are quite rare. The right panel of Figure 6 shows that the orbital period is determined to within 50% for about half of the objects. Similar uncertainties are true also for q .

In order to better evaluate the precision and reliability of our orbital period determinations we constructed a mock sample of RV measurements using orbital solutions of SB1 binaries as reported in the 9th Catalog of Spectroscopic Binaries (Pourbaix et al. 2004). For each RAVE SB1 candidate we selected its counterpart in the catalog, matching the effective temperature and dwarf nature of its primary. The orbital phase of the first RAVE observation was picked randomly, with subsequent velocities generated from the orbital solution at the same time offsets as in the actual RAVE observations. The set was processed in the same way as the RAVE observations, so that the derived orbital period could be compared to the actual one from the catalog (Figure 7). Of all objects, 50% are in the gray area, where the dispersion is $\pm 40\%$ around the true value, while 90% of all objects have periods determined to within a factor of 2. The results do not depend on the effective temperature of the primary (see the right panel in Figure 7). The results are generally acceptable but we note some

Table 3
Ranges of Parameters for Main-sequence Dwarfs

Parameter	Range	Step or Values
Angle of inclination (i)	10 ... 90 deg	Random selection of its $\sin i$ value
Eccentricity (e)	0.0 ... 0.8	0.05
Orbital period (P)	1 ... 3600 days	220 logarithmic steps
Longitude of the periastron (ω)	0 ... 360	Random selection
Mass ratio (q)	0.1 ... 0.85	0.05

Table 4
Estimated Values of Mass of the Primary Star (M_1), Mass Ratio (q), Orbital Period (P) in Days, Eccentricity (e), and System Velocity (γ) in km s^{-1}

Object	M_1/M_\odot	q	P	e	γ
J121104.5–354818	1.27	$0.45^{+0.10}_{-0.10}$	61^{+68}_{-42}	$0.25^{+0.30}_{-0.20}$	-27^{+3}_{-3}
J154304.9–122933	1.40	$0.80^{+0.05}_{-0.15}$	77^{+48}_{-59}	$0.20^{+0.30}_{-0.20}$	8^{+3}_{-3}
J021532.1–363260	1.20	$0.65^{+0.15}_{-0.15}$	49^{+15}_{-30}	$0.15^{+0.30}_{-0.15}$	48^{+2}_{-3}
J142501.1–290222	1.30	$0.80^{+0.05}_{-0.15}$	4^{+4}_{-2}	$0.00^{+0.05}_{-0.00}$	-27^{+3}_{-4}
J093202.1–083428	1.05	$0.20^{+0.15}_{-0.05}$	535^{+160}_{-262}	$0.35^{+0.20}_{-0.20}$	35^{+1}_{-1}

Note. See the text for a discussion of typical errors. In the last four columns the median values, together with lower and upper quartile limits, are reported.

(This table is available in its entirety in machine-readable form.)

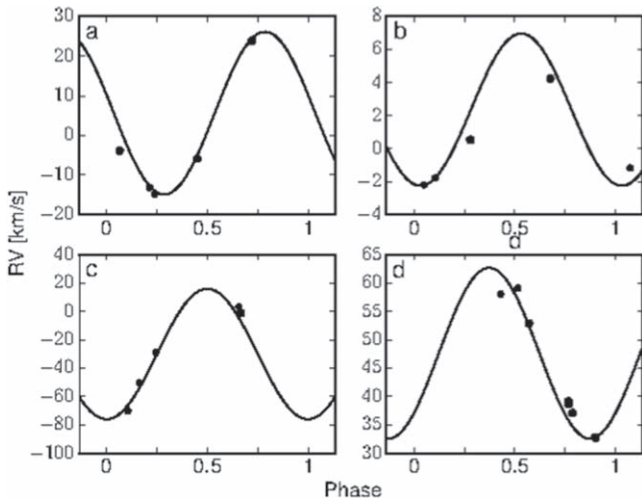


Figure 5. Examples of RV curves for a few binary systems. The black dots are RVs measured by RAVE and the curve is calculated with orbital parameters obtained with our method. The objects are J154304.9–122933 (a), J115256.0–161543 (b), J142501.1–290222 (c), and J021532.1–363260 (d).

systematics: our periods tend to be overestimated for short-period binaries and underestimated for long-period ones.

6. SB2 Candidates

SB1 candidates in RAVE have been labeled as normal single stars by a morphological classification scheme (Matijević et al. 2012). This is understandable, as the primary star is usually much brighter than the secondary one in such systems. But a close inspection of their spectra sometimes reveals a contribution of the light from the secondary, thus moving the object to the SB2 category. The signature of the secondary can be searched for in spectral lines. Due to the limited S/N ratios of the RAVE spectra the strongest lines turn out to be the most appropriate ones. So we focused on the calcium triplet lines and measured their boxiness and asymmetry indices (Figure 8). Boxiness is defined as the ratio of line widths at three quarters

and one quarter of the line depth, while asymmetry is the shift of the centroid at half maximum in units of FWHM. The reported values are averages over the three calcium lines. For a symmetric Gaussian line the boxiness equals 0.456 and the asymmetry is zero. Calcium triplet lines have broad wings, so one expects somewhat smaller values of boxiness, but the asymmetry should still be very close to zero for a spectrum of a single star, with an exception of hot stars where the presence of Paschen lines of hydrogen contaminates the wings of the calcium lines.

The combination of these values points to spectra with unusual shapes of spectral lines that could be double-lined binaries (colored dots in Figure 8). Visual inspection of those spectra confirmed the existence of several double-lined binaries where a chi-square fit with two spectra gave a much better representation of the observed spectrum than a single spectrum. List of double-lined binaries is given in the Table 5.

An example is given in Figure 9. The top panel shows five spectra of the same star, where only the last one, observed at orbital phase 0.72, shows obvious double components in the calcium triplet and also in other spectral lines. The RV curve of the same object is presented in Figure 5(a). The first four spectra in Figure 9 were obtained in 2009, while the last one, which shows double-lined spectral lines, was obtained in 2006. The bottom two panels show results of a least-square fit to this double-lined spectrum using both RVs, temperatures, mass ratio, and metallicity as free parameters, with surface gravity constrained by the assumption that both stars are on the main sequence. We note that the same solution presents a good fit also for the other four spectra, though one would expect more pronounced double-lined profiles also at the other quarter phase. This may be explained by the fact that we adopted orbital periods and phases as calculated in the SB1 fit, even though a contribution from a secondary component in SB2s may alter these values. The goal of this analysis is to point to possible SB2 candidates, but the number of multiple RAVE spectra is too small to attempt a complete solution anyway. We also note that our list of SB2 candidates contains only eight objects—these are the ones that escaped detection by the automated morphological classification algorithm (Matijević et al. 2012). On the other

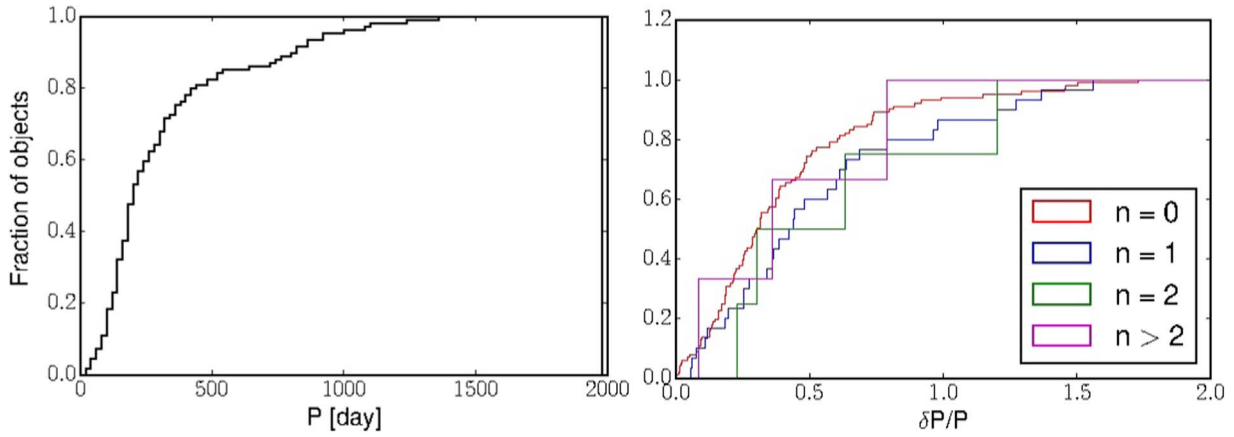


Figure 6. Left panel: cumulative diagram of estimated orbital periods. Most of the SB1 systems have periods shorter than 2 yr. Right panel: cumulative period dispersion distributions for different trends in RV changes.

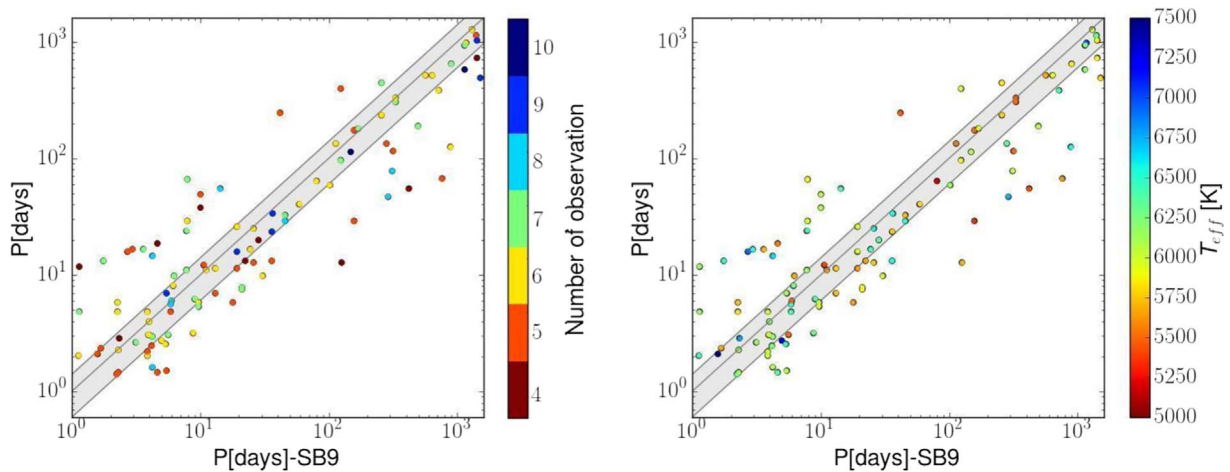


Figure 7. Comparison of true period values for objects in the 9th Catalog of Spectroscopic Binaries and for periods calculated with the method described in Section 5. The gray area represents offsets from unity of $\pm 40\%$ of the period value. The left panel is color coded by the number of observations and the right panel by the primary star's temperature. It seems that neither temperature nor the number of observations have a significant impact on our results.

hand, M. Steinmetz et al. (2019, in preparation) lists 2861 objects with (some) spectra in the SB2 category, with physical properties of 123 of them discussed already by Matijević et al. (2010).

For an object on the main sequence one could expect a moderate increase of luminosity if the object is not single but a SB1 binary system, with an effect even more pronounced for SB2s. This is an obvious consequence of an increasing contribution of light from the secondary. Indeed, the SB1s in Figure 10 are about 0.2 mag brighter than single stars, but the dispersion around the median value is the same. The data pool of SB2s is too small to make the same statistics, but it can be seen that they are brighter than single stars and some of them approach a 0.75 mag limit, which corresponds to the joint luminosity of two equal stars instead of one. The positions of evolutionary tracks of solar-type stars in Figure 10 demonstrate, however, that many of the single or binary objects may be actually evolving off the main sequence, which also makes these objects brighter. This matter is discussed in Čotar et al. (2019).

7. Combining RAVE with Gaia

The *Gaia* satellite was launched on 2013 December 19 and started with scientific observations in 2014 July (Gaia Collaboration et al. 2016). Its main objectives are astrometric

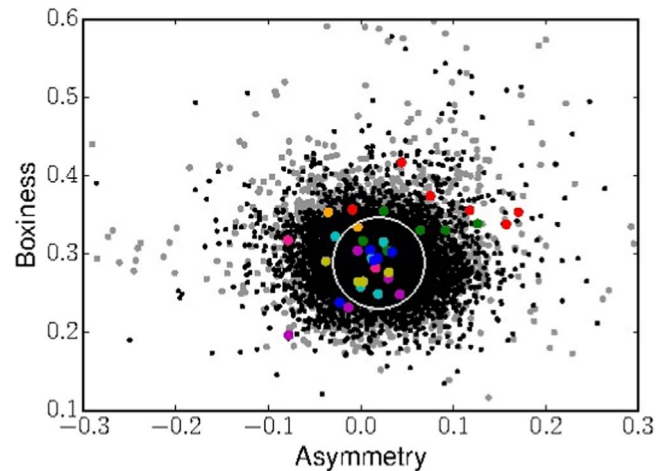


Figure 8. Asymmetry and boxiness of the calcium triplet for single stars (black dots), SB1 candidates (gray dots), and 8 SB2 candidates, each in a different color. SB1 candidates with at least one spectrum outside the marked circle with a radius of 0.05 centered on (0.01, 0.3) were visually inspected for the presence of secondary light in their spectra.

measurements of parallax and proper motion, but here we focus on results from an onboard RV spectrometer. It has a resolving power of $\sim 11,500$ covering the near-infrared wavelength

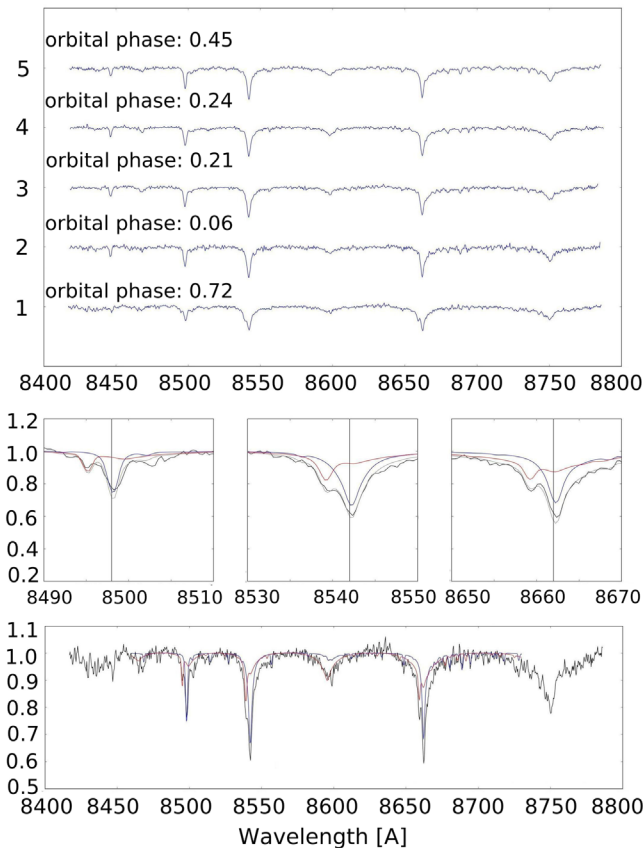


Figure 9. Top panel: spectra of the SB2 candidate J154304.9–122933 with its orbital phases labeled. The RV curve of this object is shown in Figure 5(a). Middle panel: fitted calcium triplet lines for the orbital phase 0.72. Bottom panel: fitted spectra for the same phase, using $RV_1 = -95 \text{ km s}^{-1}$, $RV_2 = 10 \text{ km s}^{-1}$, $T_1 = 7500 \text{ K}$, $T_2 = 6750 \text{ K}$, and $q = 0.55$, $[\text{Fe}/\text{H}] = 0.5$.

range at 845–782 nm, with an expected precision of 1 km s^{-1} for GK stars brighter than $G \sim 12$ (Cropper et al. 2018; Katz et al. 2019). In 2018 April the Gaia Collaboration et al. (2018) published median RVs for 7.2 million sources with effective temperatures in the range of 3550–6900 K that are brighter than $G = 12.5$. These medians were obtained over 22 months of observation (2014 July 25–2016 May 23) and have a typical overall precision of 1.05 km s^{-1} . Most of the stars observed also by RAVE lie at the faint end of objects accessible for Gaia RV measurements. For such objects ($G \sim 11.8$) the precision of Gaia RVs is 1.4 and 3.7 km s^{-1} for an effective temperature of 5000 K and 6500 K, respectively. We note that these errors are not significantly larger than for the RAVE survey, so the two sets of measurements can be efficiently combined. Indeed, for a vast majority of objects labeled as single stars in RAVE, their Gaia RV is matching closely (green solid line in Figure 11). This demonstrates that a small zero-point offset between these two data sets (estimated at 0.3 km s^{-1} ; Katz et al. 2019) does not influence our analysis when our relatively stringent limits on p_{\log} used to search for SB1 candidates are considered. Gaia DR2 published a median value of RVs and its dispersion only for objects judged to have a constant RV during the 22 months of observation. Any objects with a pronounced RV variation or SB2s were excluded. So we can expect to identify only objects with low amplitudes of RV variation which are typical for objects with long orbital periods (the black solid line in Figure 11 demonstrates that this is indeed the case). Since their

orbital periods are generally much longer than the 22 month span of the Gaia observations, it is safe to assume that all Gaia measurements were obtained at a similar orbital phase. If this was not the case one would have to consider the effects of averaging velocities at different orbital phases, which pushes their median close to system velocity. This effect is ignored in our analysis. Note that by doing so we may make a moderate underestimate of detected new SB1s, as a measurement close to system velocity dumps detected amplitudes of RV variation.

Gaia obtained its RV measurements after completion of the RAVE survey, so combining the two data sets increases the time span of RV measurements and thus allows a detection of SB1 systems with longer orbital periods. More importantly, most of its targets have been observed with RAVE only once (Figure 1), but Gaia is adding another observation and so allows testing of the variability of their RVs. In fact, Gaia itself observed each object several times, but these observations will be published only in one of the next data releases and they do not reach the combined time span of RAVE + Gaia, which stretches up to over a decade (Figure 2).

Median Gaia RVs have been calculated from several observations over 22 months. Individual measurements are not available, so we adopted an epoch of 2015 June 15, which is at the middle of the observed time span. Note that the true median epoch of Gaia RV measurements could be up to a few months earlier or later. But this has little influence on our analysis, as the closest RAVE observations were obtained at least 2.1 yr earlier. The combination of RAVE and Gaia RVs extends the maximum time span from 8 to 12 yr, while the median value is extended from 2 to 7 yr (Figure 2). We note that the use of median velocity of Gaia favors an analysis which is separate from the one based on RAVE data only.

There are 450,646 stars with RVs measured in both surveys. This is a remarkable increase by over 37,661 stars suitable for SB1 search in the RAVE-only survey. After conducting the same analysis as before (Section 3) we obtained the following results. Of the stars with observations in both data sets 7.7% are SB1 candidates. This is close to a the fraction of 10.2% that was obtained based on RAVE data only, even though the time span is much longer. Among RAVE stars with multiple observations that were labeled as single stars ($p_{\log} < 2.87$) we found almost 10% new binary candidates after we included Gaia velocities in calculations. Overall, we were able to identify 27,716 SB1 candidates in the RAVE + Gaia sample, compared to 3838 from the RAVE-only analysis.

The black dashed line in Figure 11 shows the RV variability for stars that were classified as normal single stars, according to their RAVE RVs. For the vast majority of objects the RV changes are less than 5 km s^{-1} , so we can assume those objects are long-period binaries, impossible to detect without observations over a longer time span. After we added Gaia velocities, the resulting RV variability became significant for some of these stars and we identified new SB1 candidates. Future Gaia data releases will probably reveal even more binary candidates.

Next we repeated the computation of orbital parameters (Section 5), now adding Gaia velocities. The results are shown in Figure 12. The results are very similar as for the RAVE-only data set. This is a consequence of the similar accuracy of RV measurements in both samples. Median values together with lower and upper quartile limits are reported in Table 7. More than 90% of objects have all of the derived parameters with combination of the Rave and Gaia velocities in the interquartile

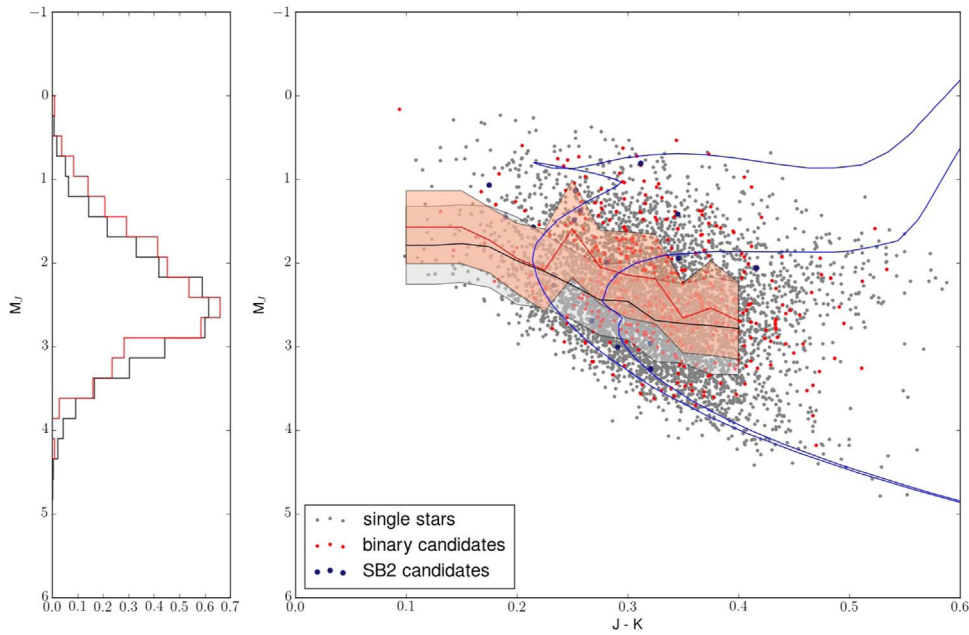


Figure 10. Absolute magnitude–color diagram for single, SB1, and SB2 candidate stars. The blue lines are 2 and 4 Gyr Padova isochrones (Marigo et al. 2017) with a metallicity set to the solar value. Gray dots are RAVE single stars, red ones are SB1 candidates, and black ones SB2 candidates. The black solid line is the median value of the J magnitude for single stars and the gray area indicates the σ around median. Similarly, red solid line and shaded area are medians for SB1 candidates.

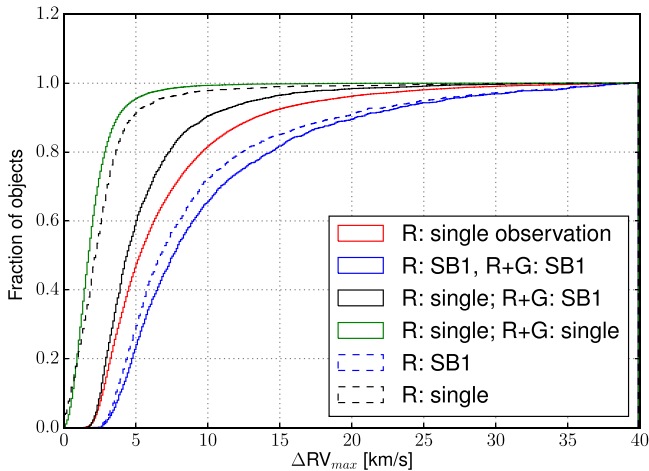


Figure 11. Maximum RV variability for groups of objects identified as single stars or SB1 candidates by the RAVE DR6 survey alone (label R), or by a combination of the RAVE and *Gaia* DR2 (label R + G) surveys. The red line denotes RV differences between RAVE and *Gaia* for all objects that have only one RAVE observation. The green line shows that the RVs of single stars match to $\sim 2 \text{ km s}^{-1}$ across the surveys, so one can use a combination of RVs from both surveys to search for SB1 candidates. The black solid line demonstrates that a combination of the two surveys can use its long time span to identify SB1s with the lowest RV amplitude.

range (between upper and lower quartiles) of RAVE-only data set.

8. Conclusions

This paper presents a complete list of SB1 candidate stars in the RAVE survey based on the requirement that their RV measurements differ by at least $\sim 4.2\sigma$ apart ($p_{\log} = 2.87$). Using the probability function described in Matijevič et al. (2011) we detected 3838 single-lined spectroscopic binary candidates. This almost triples the number of candidates known

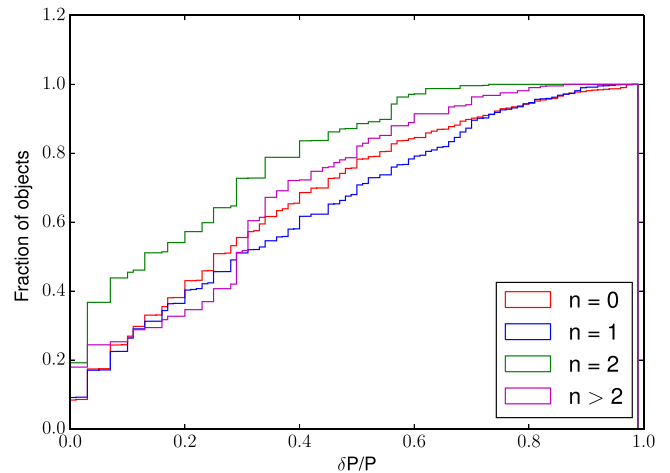


Figure 12. Cumulative histogram of the relative dispersion of period median values for SB1 candidates with RAVE DR5 + *Gaia* DR2 velocities combined. The results are similar to the ones with RAVE DR6 data only (Figure 6). About 70% of the objects have P determined to within 50%.

Table 5

Most Probable Values of Parameters for Double-lined Binary Candidates: Mass Ratio (q), Temperature of Primary (T_1), Temperature of Secondary Star (T_2), and Metallicity [Fe/H]

Object	q	T_1	T_2	[Fe/H]
J120432.1–203723	0.5	7250	6750	0.5
J203415.1–201303	0.6	6750	6500	−0.5
J090701.4–142256	0.65	4750	4500	0.0
J125113.4–202156	0.5	7500	6750	−0.5
J154304.9–122933	0.55	7500	6750	−0.5
J161301.0–130342	0.65	5000	4750	−0.5
J100235.9–093818	0.55	7000	6250	−0.5
J045419.4–030709	0.55	6750	6000	−0.5

Table 6
Representative Sample from the Full Online List of SB1 Candidates Obtained by a Combination of RAVE and *Gaia* RV Measurements

Object	p_{\log}	N obs	Time Span	Epoch (first)	Epoch (last)
J012955.0–623622	5.99	3	2462	2008 Sep 17	2015 Jun 15
J135416.6–222607	4.30	3	3758	2005 Mar 1	2015 Jun 15
J004904.6–222139	8.91	3	4262	2003 Oct 14	2015 Jun 15
J070727.9–480148	11.56	4	3126	2006 Nov 23	2015 Jun 15
J051516.8–324737	5.53	3	3423	2006 Jan 30	2015 Jun 15

Note. The table is similar to Table 2 but it contains a much larger list of 27,716 SB1 candidates. The complete table is available electronically. An epoch of 2015 June 15 for the *Gaia* observations was adopted (see Section 7 for an explanation).

(This table is available in its entirety in machine-readable form.)

so far and corresponds to $\sim 10\%$ of all normal stars observed multiple times by RAVE. Most of the primary stars of these systems belong to main-sequence dwarfs with temperatures around 6000 K and masses around 1–1.2 M_{\odot} , or red clump stars and red giant stars with temperatures of 4500–5000 K and masses larger than 1.5 M_{\odot} . The secondary stars contribute only a small fraction of the total light of an SB1 candidate. Still, the spectral lines in the combined spectrum are somewhat shallower, so this may be the reason why SB1 candidates appear to be more metal-poor than the general RAVE population.

Even though most of the stars with repeated observations in RAVE have been observed only a few times, it is possible to make a rough estimate of the orbital parameters for systems with primary components on the main sequence. We focused on systems with at least four observations. Being limited by the time span between re-observations, our results showed that most systems have an orbital period shorter than one year, and only a few of them have orbital periods of around three years.

Our sample of SB1 candidates includes stars morphologically classified as normal single stars. But at least in some cases one may hope to identify a contribution of the secondary component to the total light of the system. In the spectra this is revealed by unusual shapes of the spectral lines, which were measured through the boxiness and asymmetry of calcium triplet lines. A visual inspection of their spectra revealed some compelling cases with a mass ratio around 0.8. We also note that both SB1 and SB2 candidates tend to be somewhat brighter than their single-star counterparts, which is consistent with a contribution of light from a secondary component.

Gaia DR2 is supplementing the RAVE data set with another RV observation for 450,646 stars. It also observed at an epoch after RAVE observations were concluded, so the combined data set has a larger time span of up to 12 yr and with a median of 7 yr. The analysis of the combined data sets allows us to identify 27,716 stars as single-lined binary candidates, which presents an order of magnitude increase over earlier studies. The orbital and physical properties of these systems are similar to the ones from the RAVE-only data set, but an accurate knowledge of their spatial position and velocity vectors provided by *Gaia* DR2 allows us to calculate their Galactic orbits and to further characterize their physical parameters.

The contents of Tables 6 and 7 are available in electronic edition.

We thank the anonymous referee for useful comments which improved the clarity of the manuscript. Funding for RAVE has

Table 7

Estimated Values of the Mass Ratio (q), Orbital Period (P) in Days, Eccentricity (e), and System Velocity (γ) in km s^{-1} with Lower and Upper Quartile Limits for the Combination of the RAVE and the *Gaia* Surveys

Object	q	P	e	γ
J121104.5–354818	0.45 $^{+0.15}_{-0.10}$	92 $^{+52}_{-73}$	0.25 $^{+0.35}_{-0.25}$	–19 $^{+2}_{-2}$
J154304.9–122933	0.80 $^{+0.05}_{-0.15}$	77 $^{+48}_{-59}$	0.40 $^{+0.25}_{-0.35}$	6 $^{+3}_{-4}$
J021532.1–363260	0.65 $^{+0.15}_{-0.15}$	49 $^{+15}_{-30}$	0.15 $^{+0.25}_{-0.15}$	49 $^{+3}_{-2}$
J142501.1–290222	0.80 $^{+0.05}_{-0.15}$	4 $^{+4}_{-2}$	0.00 $^{+0.05}_{-0.00}$	–33 $^{+4}_{-4}$
J093202.1–083428	0.20 $^{+0.20}_{-0.05}$	341 $^{+257}_{-107}$	0.45 $^{+0.15}_{-0.25}$	35 $^{+1}_{-1}$

(This table is available in its entirety in machine-readable form.)

been provided by: the Leibniz-Institut für Astrophysik Potsdam (AIP); the Australian Astronomical Observatory; the Australian National University; the Australian Research Council; the French National Research Agency; the German Research Foundation (SPP 1177 and SFB 881); the European Research Council (ERC-StG 240271 Galactica); the Istituto Nazionale di Astrofisica at Padova; The Johns Hopkins University; the National Science Foundation of the USA (AST-0908326); the W. M. Keck foundation; the Macquarie University; the Netherlands Research School for Astronomy; the Natural Sciences and Engineering Research Council of Canada; the Slovenian Research Agency (core funding No. P1-0188); the Swiss National Science Foundation; the Science & Technology Facilities Council of the UK; Opticon; Strasbourg Observatory; and the Universities of Basel, Groningen, Heidelberg and Sydney. T.Z. thanks the Research School of Astronomy & Astrophysics in Canberra for support through a Distinguished Visitor Fellowship.

This work has made use of data from the European Space Agency (ESA) mission *Gaia* (<https://www.cosmos.esa.int/gaia>), processed by the *Gaia* Data Processing and Analysis Consortium (DPAC; <https://www.cosmos.esa.int/web/gaia/dpac/consortium>). Funding for the DPAC has been provided by national institutions, in particular the institutions participating in the *Gaia* Multilateral Agreement.

ORCID iDs

Danijela Birko  <https://orcid.org/0000-0002-5571-5981>
Tomaž Zwitter  <https://orcid.org/0000-0002-2325-8763>
Georges Kordopatis  <https://orcid.org/0000-0002-9035-3920>
Joss Bland-Hawthorn  <https://orcid.org/0000-0001-7516-4016>
Guillaume Guiglion  <https://orcid.org/0000-0002-1317-2798>

Brad K. Gibson  <https://orcid.org/0000-0003-4446-3130>
 Matthias Steinmetz  <https://orcid.org/0000-0001-6516-7459>

References

- Abt, H. A., & Willmarth, D. W. 1999, *ApJ*, 521, 682
 Čotar, K., Zwitter, T., Traven, G., et al. 2019, *MNRAS*, 487, 2474
 Cropper, M., Katz, D., Sartoretti, P., et al. 2018, *A&A*, 616, A5
 De Silva, G. M., Freeman, K. C., Bland-Hawthorn, J., et al. 2015, *MNRAS*, 449, 2604
 Duquennoy, A., & Mayor, M. 1991, *A&A*, 500, 337
 Fischer, D. A., & Marcy, G. W. 1992, *ApJ*, 396, 178
 Gaia Collaboration, Brown, A. G. A., Vallenari, A., et al. 2018, *A&A*, 616, A1
 Gaia Collaboration, Prusti, T., de Bruijne, J. H. J., et al. 2016, *A&A*, 595, A1
 Gilmore, G., Randich, S., Asplund, M., et al. 2012, *Msngr*, 147, 25
 Griffin, R. F. 2006, *MNRAS*, 371, 1159
 Holtzman, J. A., Shetrone, M., Johnson, J. A., et al. 2015, *AJ*, 150, 148
 Katz, D., Sartoretti, P., Cropper, M., et al. 2019, *A&A*, 622, A205
 Kordopatis, G., Gilmore, G., Steinmetz, M., et al. 2013, *AJ*, 146, 134
 Kos, J., Zwitter, T., Wyse, R., et al. 2014, *Sci*, 345, 791
 Kunder, A., Kordopatis, G., Steinmetz, M., et al. 2017, *AJ*, 153, 75
 Latham, D. W., Stefanik, R. P., Torres, G., et al. 2002, *AJ*, 124, 1144
 Liu, C., Xu, Y., Wan, J.-C., et al. 2017, *RAA*, 17, 096
 Marigo, P., Girardi, L., Bressan, A., et al. 2017, *ApJ*, 835, 77
 Matijevič, G., Zwitter, T., Bienaymé, O., et al. 2011, *AJ*, 141, 200
 Matijevič, G., Zwitter, T., Bienaymé, O., et al. 2012, *ApJS*, 200, 14
 Matijevič, G., Zwitter, T., Munari, U., et al. 2010, *AJ*, 140, 184
 Mermilliod, J. C., Andersen, J., Latham, D. W., & Mayor, M. 2007, *A&A*, 473, 829
 Munari, U., Tomasella, L., Fiorucci, M., et al. 2008, *A&A*, 488, 969
 Nordström, B., Mayor, M., Andersen, J., et al. 2004, *A&A*, 418, 989
 Pourbaix, D., Knapp, G. R., Szkody, P., et al. 2005, *A&A*, 444, 643
 Pourbaix, D., Tokovinin, A. A., Batten, A. H., et al. 2004, *A&A*, 424, 727
 Raghavan, D., McAlister, H. A., Henry, T. J., et al. 2010, *ApJS*, 190, 1
 Sana, H., Gosset, E., & Evans, C. J. 2009, *MNRAS*, 400, 1479
 Siebert, A., Williams, M. E. K., Siviero, A., et al. 2011, *AJ*, 141, 187
 Sommariva, V., Piotto, G., Rejkuba, M., et al. 2009, *A&A*, 493, 947
 Steinmetz, M., Zwitter, T., Siebert, A., et al. 2006, *AJ*, 132, 1645
 Wojno, J., Kordopatis, G., Piffl, T., et al. 2017, *MNRAS*, 468, 3368
 Žerjal, M., Zwitter, T., Matijevič, G., et al. 2013, *ApJ*, 776, 127
 Zwitter, T., Siebert, A., Munari, U., et al. 2008, *AJ*, 136, 421